

Selective Inference for Testing Trees and Edges in Phylogenetics

Hidetoshi Shimodaira^{1,3} and Yoshikazu Terada^{2,3}

shimo@i.kyoto-u.ac.jp and terada@sigmath.es.osaka-u.ac.jp

¹*Graduate School of Informatics, Kyoto University, Yoshida Honmachi, Sakyo-ku, Kyoto, 606-8501, Japan*

²*Graduate School of Engineering Science, Osaka University, 1-3 Machikaneyama-cho, Toyonaka, Osaka 560-8531, Japan*

³*Mathematical Statistics Team, RIKEN Center for Advanced Intelligence Project, 1-4-1 Nihonbashi, Chuo-ku, Tokyo 103-0027, Japan*

Abstract:

Selective inference is considered for testing trees and edges in phylogenetic tree selection from molecular sequences. This improves the previously proposed approximately unbiased test by adjusting the selection bias when testing many trees and edges at the same time. The newly proposed selective inference p -value is useful for testing selected edges to claim that they are significantly supported if $p > 1 - \alpha$, whereas the non-selective p -value is still useful for testing candidate trees to claim that they are rejected if $p < \alpha$. The selective p -value controls the type-I error conditioned on the selection event, whereas the non-selective p -value controls it unconditionally. The selective and non-selective approximately unbiased p -values are computed from two geometric quantities called signed distance and mean curvature of the region representing tree or edge of interest in the space of probability distributions. These two geometric quantities are estimated by fitting a scaling-law model to the non-parametric multiscale bootstrap probabilities. For better understanding the geometric nature of the problem, a visualization of probability distributions is presented. Our general method is applicable to a wider class of problems; phylogenetic tree selection is an example of model selection, and it is interpreted as the variable selection of multiple regression, where each edge corresponds to each predictor. Our method is illustrated in a previously controversial phylogenetic analysis of human, rabbit and mouse.

Keywords and phrases: Statistical hypothesis testing, Multiple testing, Selection bias, Model selection, Akaike information criterion, Bootstrap resampling, Hierarchical clustering, Variable selection.

1. Introduction

For illustrating the idea of *selective inference*, we first look at a simple example of 1-dimensional normal random variable Z with unknown mean $\theta \in \mathbb{R}$ and variance 1:

$$Z \sim N(\theta, 1). \quad (1)$$

Observing $Z = z$, we would like to test the null hypothesis $H_0 : \theta \leq 0$ against the alternative hypothesis $H_1 : \theta > 0$. The ordinary (i.e., non-selective) inference leads to the p -value of the one-tailed z -test as

$$p(z) := P(Z > z \mid \theta = 0) = \bar{\Phi}(z), \quad (2)$$

where $\bar{\Phi}(x) = 1 - \Phi(x) = \Phi(-x)$ and $\Phi(x)$ is the cumulative distribution function of $N(0, 1)$. What happens when we test many hypotheses at the same time? Consider random variables $Z_i \sim N(\theta_i, 1)$, $i = 1, \dots, K_{\text{all}}$, not necessarily independent, with null hypotheses $\theta_i \leq 0$. For dealing with the multiplicity of testing, there are several approaches such as the family-wise error rate (FWER) and the false discovery rate (FDR), and here selective inference (SI) is discussed as a yet another approach. Instead of testing all the K_{all} hypotheses, we select K_{select} hypotheses with $z_i > c_i$ for constants c_i specified in advance. This kind of selection is very common in practice (e.g., publication bias), and it is called as the *file drawer problem* by Rosenthal (1979). Instead of controlling the multiplicity of testing, SI alleviates it by reducing the number of tests. The mathematical formulation of SI is easier than FWER and FDR in the sense that each hypothesis can be considered separately. For one of hypotheses, we simply write $z > c$ by dropping the index i . In selective inference, we consider conditional probability given the selection event, which leads to the following p -value (Fithian, Sun and Taylor, 2014; Tian and Taylor, 2018)

$$p(z, c) := P(Z > z \mid Z > c, \theta = 0) = \bar{\Phi}(z)/\bar{\Phi}(c), \quad (3)$$

where the selection bias is adjusted by dividing $p(z)$ by the selection probability $\bar{\Phi}(c)$; in the case of $c = 0$, this corresponds to the two-tailed z -test, because the selection probability is $\bar{\Phi}(0) = 0.5$ and $p(z, c) = 2p(z)$. For significance level α (we use $\alpha = 0.05$ throughout the paper), it properly controls the type-I error conditioned on the selection event as $P(p(Z, c) < \alpha \mid Z > c, \theta = 0) = \alpha$, while the non-selective p -value violates the type-I error as $P(p(Z) < \alpha \mid Z > c, \theta = 0) = \alpha/\bar{\Phi}(c) > \alpha$. The selection bias can be very large when $\bar{\Phi}(c) \ll 1$ (i.e. $c \gg 0$), or $K_{\text{select}} \ll K_{\text{all}}$.

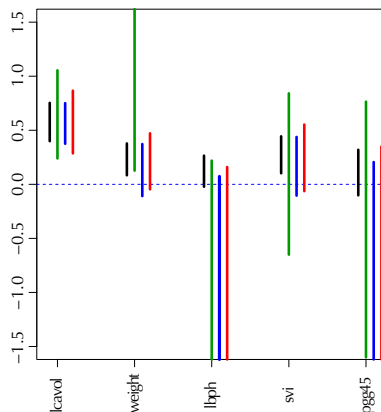


FIG 1. Confidence intervals of regression coefficients for selected variables by lasso; see Section 6.7 for details. (Black) the ordinary confidence interval $[L_j^{\text{ordinary}}, U_j^{\text{ordinary}}]$. (Green) the selective confidence interval $[L_j^{\text{model}}, U_j^{\text{model}}]$ under the selected model. (Blue) the selective confidence interval $[L_j^{\text{variable}}, U_j^{\text{variable}}]$ under the selection event that variable j is selected. (Red) its approximation $[\hat{L}_j^{\text{variable}}, \hat{U}_j^{\text{variable}}]$ computed by the multiscale bootstrap method.

Selective inference has been mostly developed for inferences after model selection (Taylor and Tibshirani, 2015; Tibshirani et al., 2016), particularly variable selection in regression settings such as lasso (Tibshirani, 1996). Recently, Terada and Shimodaira (2017) developed a general method for selective inference by adjusting the selection bias in the approximately unbiased (AU) p -value computed by the multiscale bootstrap method (Shimodaira, 2002, 2004, 2008). This new method can be used to compute, for example, confidence intervals of regression coefficients in lasso (figure 1). In this paper, we apply this method to phylogenetic inference for computing proper confidence levels of tree topologies (dendrograms) and edges (clades or clusters) of species. As far as we know, this is the first attempt to consider selective inference in phylogenetics. Our selective inference method is implemented in software *scaleboot* (Shimodaira, 2019) working jointly with *CONSEL* (Shimodaira and Hasegawa, 2001) for phylogenetics, and it is also implemented in a new version of *pvclust* (Suzuki and Shimodaira, 2006) for hierarchical clustering, where only edges appeared in the observed tree are “selected” for computing p -values. Although our argument is based on the rigorous theory of mathematical statistics in Terada and Shimodaira (2017), a self-contained illustration is presented in this paper for the theory as well as the algorithm of selective inference.

Phylogenetic tree selection is an example of model selection. Since each tree can be specified as a combination of edges, tree selection can be interpreted as the variable selection of multiple regression, where edges correspond to the predictors of regression (Shimodaira,

2001; Shimodaira and Hasegawa, 2005). We simply compare the log-likelihood values of trees for finding the maximum likelihood (ML) tree (Felsenstein, 1981), because all the candidate trees have the same number of model parameters. In order to adjust the model complexity by the number of parameters in general model selection, we compare Akaike Information Criterion (AIC) values of candidate models (Akaike, 1974). AIC is used in phylogenetics for selecting the substitution model (Posada and Buckley, 2004). There are modifications of AIC for more precise estimation of the complexity term (Burnham and Anderson, 2002; Konishi and Kitagawa, 2008, known as Takeuchi Information Criterion), that for incomplete data (Shimodaira and Maeda, 2018), or that for the covariate-shift data (Shimodaira, 2000). AIC and all these modifications are derived for estimating the expected Kullback-Leibler divergence between the unknown true distribution and the estimated probability distribution on the premise that the model is misspecified. When using regression model for prediction purpose, it may be sufficient to find only the best model which minimizes the AIC value. Considering random variations of dataset, however, it is obvious in phylogenetics that the ML tree does not necessarily represent the true history of evolution. Therefore, Kishino and Hasegawa (1989) proposed a statistical test whether two log-likelihood values differ significantly (also known as *Kishino-Hasegawa* test). The log-likelihood difference is often not significant, because its variance can be very large for non-nested models when the divergence between two probability distributions is large; see eq. (26) in Section 6.1. The same idea of model selection test whether two AIC values differ significantly has been proposed independently in statistics (Linhart, 1988) and econometrics (Vuong, 1989). For comparing two regression models, the model selection test is already discussed in Efron (1984) with a bootstrap method to compute a confidence interval corresponding to the AU p -value (Shimodaira, 2002). For testing which model is better than the other, the null hypothesis in the model selection test is that the two models are equally good in terms of the expected value of AIC on the premise that both models are misspecified. The model selection test is very different from the classical setting, such as the likelihood ratio test for nested models and the modified likelihood ratio test for non-nested models (Cox, 1962), for testing whether the model is correctly specified or not. In order to construct the confidence set of models, a multiple comparisons method is introduced for comparing AIC values of more than two models (Shimodaira, 1998; Shimodaira and Hasegawa, 1999). But it is conservative by nature, leading to more false negatives than expected, because it considers the worst scenario, called the least favorable configuration. On the other hand, the model selection test and bootstrap probability (Felsenstein, 1985) lead to more false positives than expected when comparing

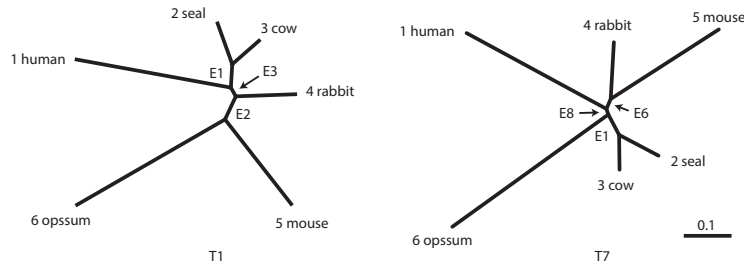


FIG 2. Examples of two unrooted trees $T1$ and $T7$. Branch lengths represent ML estimates of parameters (expected number of substitutions per site). $T1$ includes edges $E1$, $E2$ and $E3$, and $T7$ includes $E1$, $E6$ and $E8$.

more than two models (Shimodaira, 2002). The AU p -value mentioned earlier has been developed for solving this problem, and we are going to upgrade it for selective inference.

2. Phylogenetic Inference

As a working example, we estimate phylogenetic tree from the same dataset previously analyzed in Shimodaira and Hasegawa (1999); Shimodaira (2001, 2002) using the same model of evolution. The dataset consists of mitochondrial protein sequences of six mammalian species with $n = 3414$ amino acids (n is treated as sample size). The taxa are labelled as 1=*Homo sapiens* (human), 2=*Phoca vitulina* (seal), 3=*Bos taurus* (cow), 4=*Oryctolagus cuniculus* (rabbit), 5=*Mus musculus* (mouse), and 6=*Didelphis virginiana* (opossum). The dataset will be denoted as $\mathcal{X}_n = (\mathbf{x}_1, \dots, \mathbf{x}_n)$. The software package PAML (Yang, 1997) was used to calculate the site-wise log-likelihoods for trees. The mtREV model (Adachi and Hasegawa, 1996) was used for amino acid substitutions, and the site-heterogeneity was modeled by the discrete-gamma distribution (Yang, 1996).

The number of unrooted trees for six taxa is 105. These trees are reordered by their likelihood values and labelled as $T1, T2, \dots, T105$. $T1$ is the ML tree as shown in figure 2 and its tree topology is represented as $((((1(23))4)5)6)$. There are three internal branches (we call them as edges) in $T1$, which are labelled as $E1, E2$ and $E3$. For example, $E1$ splits the six taxa as $\{23|1456\}$ and the partition of six taxa is represented as $-++---$, where $+/-$ indicates taxa 1, $\dots, 6$ from left to right and $++$ indicates the clade $\{23\}$ (we set $-$ for taxon 6, since it is treated as the outgroup). There are 25 edges in total, and each tree is specified by selecting three edges from them, although not all the combinations of three edges are allowed.

The result of phylogenetic analysis is summarized in table 1 for trees and table 2 for

A Projection of data point X to tree models

B Regions for trees with data point X

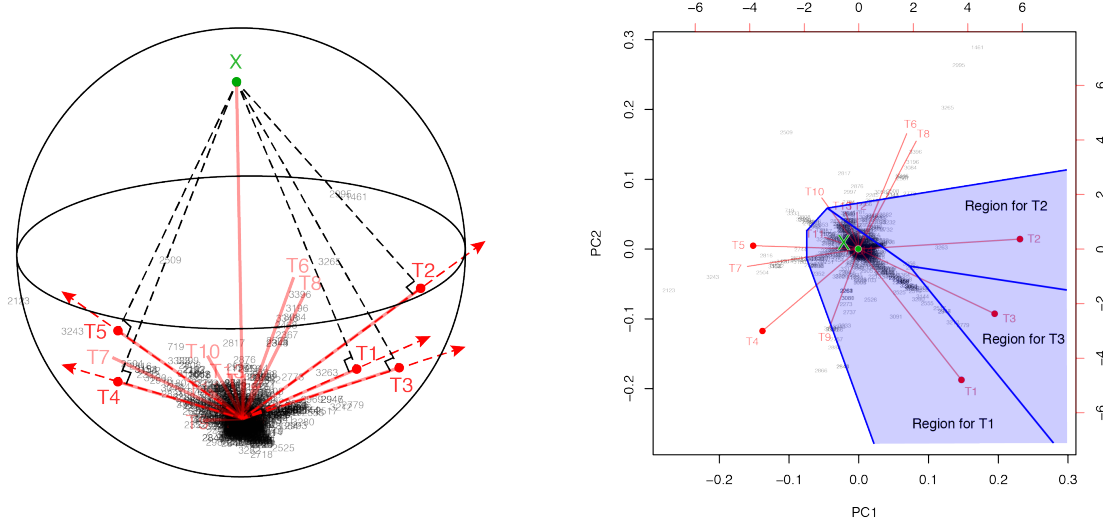


FIG 3. Model map: Visualization of ML estimates of probability distributions for the best 15 trees. The origin represents the star-shaped tree topology (obtained by reducing the internal branches to zero length). Sites of amino acid sequences $t = 1, \dots, n$ (black numbers) and probability distributions for trees $T1, \dots, T15$ (red segments) are drawn by biplot of PCA. Auxiliary lines are drawn by hand. (A) 3-dimensional visualization using PC1, PC2 and PC3. The reconstructed data point X is also shown (green point). The ML estimates are represented as the end points of the red segments (shown by red points only for the best five trees), and they are placed on the sphere with the origin and X being placed at the poles. (B) The top-view of model map. Regions for the best three trees T_i , $i = 1, 2, 3$ (blue shaded regions) are illustrated; T_i will be the ML tree if X is included in the region for T_i .

TABLE 1

Three types of p -values (BP, AU, SI) and geometric quantities (β_0, β_1) for the best 20 trees. Standard errors are shown in parentheses. Boldface indicates significance ($p < 0.05$) for the null hypothesis that the tree is true. For the rest of trees ($T21, \dots, T105$), p -values are very small ($p < 0.001$).

tree	BP	AU	SI	β_0	β_1	topology	edges
T1 [†]	0.559 (0.001)	0.752 (0.001)	0.372 (0.001)	-0.41 (0.00)	0.27 (0.00)	(((1(23))4)5)6	E1,E2,E3
T2	0.304 (0.000)	0.467 (0.001)	0.798 (0.001)	0.30 (0.00)	0.22 (0.00)	(((1(23)4)5)6)	E1,E2,E4
T3	0.038 (0.000)	0.126 (0.002)	0.202 (0.003)	1.46 (0.01)	0.32 (0.00)	(((14)(23))5)6	E1,E2,E5
T4	0.014 (0.000)	0.081 (0.002)	0.124 (0.003)	1.79 (0.01)	0.40 (0.01)	((1(23))(45)6)	E1,E3,E6
T5	0.032 (0.000)	0.127 (0.002)	0.199 (0.003)	1.50 (0.01)	0.36 (0.00)	1((23)(45)6)	E1,E6,E7
T6	0.005 (0.000)	0.032 (0.002)	0.050 (0.002)	2.21 (0.02)	0.35 (0.01)	1(((23)4)5)6)	E1,E4,E7
T7 [‡]	0.015 (0.000)	0.100 (0.003)	0.150 (0.003)	1.72 (0.01)	0.44 (0.01)	((1(45))(23)6)	E1,E6,E8
T8	0.001 (0.000)	0.011 (0.001)	0.016 (0.002)	2.74 (0.03)	0.43 (0.02)	((15)(23)4)6)	E1,E4,E9
T9	0.000 (0.000)	0.001 (0.000)	0.001 (0.000)	3.67 (0.09)	0.46 (0.04)	(((1(23))5)4)6)	E1,E3,E10
T10	0.002 (0.000)	0.022 (0.002)	0.033 (0.002)	2.43 (0.02)	0.42 (0.01)	(((15)4)(23)6)	E1,E8,E9
T11	0.000 (0.000)	0.004 (0.001)	0.006 (0.002)	3.14 (0.07)	0.51 (0.03)	(((14)5)(23)6)	E1,E5,E8
T12	0.000 (0.000)	0.000 (0.000)	0.001 (0.000)	3.78 (0.09)	0.41 (0.04)	(((15)(23))4)6)	E1,E9,E10
T13	0.000 (0.000)	0.000 (0.000)	0.001 (0.001)	3.96 (0.19)	0.54 (0.09)	1(((23)5)4)6)	E1,E7,E11
T14	0.000 (0.000)	0.000 (0.000)	0.000 (0.000)	4.66 (0.31)	0.65 (0.12)	((14)((23)5)6)	E1,E5,E11
T15	0.000 (0.000)	0.000 (0.000)	0.000 (0.000)	5.28 (0.34)	0.43 (0.11)	((1(23)5)4)6)	E1,E10,E11
T16	0.000 (0.000)	0.000 (0.000)	0.001 (0.000)	3.63 (0.04)	0.23 (0.01)	(((13)2)4)5)6)	E2,E3,E12
T17	0.000 (0.000)	0.000 (0.000)	0.000 (0.000)	3.81 (0.04)	0.22 (0.01)	(((12)3)4)5)6)	E2,E3,E13
T18	0.000 (0.000)	0.000 (0.000)	0.000 (0.000)	4.33 (0.10)	0.34 (0.03)	(((13)2)(45)6)	E3,E6,E12
T19	0.000 (0.000)	0.000 (0.000)	0.000 (0.000)	4.36 (0.11)	0.32 (0.04)	(((12)3)(45)6)	E3,E6,E13
T20	0.000 (0.000)	0.000 (0.000)	0.000 (0.000)	3.90 (0.12)	0.44 (0.05)	(((1(45))2)3)6)	E6,E8,E14

[†] T1 is the ML tree, i.e., the tree selected by the ML method based on the dataset of Shimodaira and Hasegawa (1999). [‡] T7 is presumably the true tree as suggested by later researches; see Section 4.3.

TABLE 2

Three types of p -values (BP, AU, SI) and geometric quantities (β_0, β_1) for all the 25 edges of six taxa. Standard errors are shown in parentheses. Boldface without underline indicates significance ($p < 0.05$) for the null hypothesis that the edge is true. Boldface with underline indicates significance ($p > 0.95$) for the null hypothesis that the edge is not true.

edge	BP	AU	SI	β_0	β_1	clade
E1 ^{†‡}	1.000 (0.000)	1.000 (0.000)	1.000 (0.000)	-3.87 (0.03)	0.16 (0.01)	-----
E2 [†]	0.930 (0.000)	0.956 (0.001)	0.903 (0.001)	-1.59 (0.00)	0.12 (0.00)	+++++
E3 [†]	0.580 (0.001)	0.719 (0.001)	0.338 (0.001)	-0.39 (0.00)	0.19 (0.00)	+++++
E4	0.318 (0.000)	0.435 (0.001)	0.775 (0.001)	0.32 (0.00)	0.16 (0.00)	+++++
E5	0.037 (0.000)	0.124 (0.002)	0.198 (0.002)	1.47 (0.01)	0.32 (0.00)	+++++
E6 [‡]	0.060 (0.000)	0.074 (0.001)	0.141 (0.002)	1.50 (0.00)	0.05 (0.00)	-----
E7	0.038 (0.000)	0.091 (0.002)	0.154 (0.002)	1.56 (0.01)	0.22 (0.00)	+++++
E8 [‡]	0.018 (0.000)	0.068 (0.002)	0.110 (0.003)	1.80 (0.01)	0.31 (0.01)	+++++
E9	0.003 (0.000)	0.014 (0.001)	0.023 (0.002)	2.48 (0.02)	0.27 (0.02)	+++++
E10	0.000 (0.000)	0.000 (0.000)	0.001 (0.000)	3.72 (0.07)	0.29 (0.03)	+++++
E11	0.000 (0.000)	0.000 (0.000)	0.000 (0.000)	4.31 (0.10)	0.35 (0.03)	+++++
E12	0.000 (0.000)	0.000 (0.000)	0.000 (0.000)	3.68 (0.05)	0.17 (0.02)	+++++
E13	0.000 (0.000)	0.000 (0.000)	0.000 (0.000)	3.90 (0.04)	0.15 (0.02)	+++++
E14	0.000 (0.000)	0.000 (0.000)	0.000 (0.000)	4.03 (0.09)	0.30 (0.04)	+++++
E15	0.000 (0.000)	0.000 (0.000)	0.000 (0.000)	4.03 (0.13)	0.38 (0.06)	+++++
E16	0.000 (0.000)	0.000 (0.000)	0.000 (0.000)	4.44 (0.05)	0.12 (0.01)	+++++
E17	0.000 (0.000)	0.000 (0.000)	0.000 (0.000)	4.70 (0.07)	0.19 (0.02)	+++++
E18	0.000 (0.000)	0.000 (0.000)	0.000 (0.000)	3.94 (0.09)	0.26 (0.04)	+++++
E19	0.000 (0.000)	0.000 (0.000)	0.000 (0.000)	5.23 (0.43)	0.57 (0.13)	+++++
E20	0.000 (0.000)	0.000 (0.000)	0.000 (0.000)	5.66 (0.29)	0.28 (0.09)	+++++
E21	0.000 (0.000)	0.000 (0.000)	0.000 (0.000)	6.38 (0.33)	0.24 (0.08)	+++++
E22	0.000 (0.000)	0.000 (0.000)	0.000 (0.000)	5.62 (0.21)	0.17 (0.07)	+++++
E23	0.000 (0.000)	0.000 (0.000)	0.000 (0.000)	4.86 (0.43)	0.70 (0.13)	+++++
E24	0.000 (0.000)	0.000 (0.000)	0.000 (0.000)	5.61 (0.17)	0.23 (0.04)	+++++
E25	0.000 (0.000)	0.000 (0.000)	0.000 (0.000)	6.32 (0.71)	0.52 (0.20)	+++++

[†] Edges included in T1. [‡] Edges included in T7.

edges. Three types of p -values are computed for each tree as well as for each edge. BP is the bootstrap probability (Felsenstein, 1985) and AU is the approximately unbiased p -value (Shimodaira, 2002). Bootstrap probabilities are computed by the non-parametric bootstrap resampling (Efron, 1979) described in Section 6.1. The theory and the algorithm of BP and AU will be reviewed in Section 3. Since we are testing many trees and edges at the same time, there is potentially a danger of selection bias. The issue of selection bias has been discussed in Shimodaira and Hasegawa (1999) for introducing the method of multiple comparisons of log-likelihoods (also known as *Shimodaira-Hasegawa test*) and in Shimodaira (2002) for introducing AU test. However, these conventional methods are only taking care of the multiplicity in computing one p -value instead of many p -values at the same time. Therefore, we intend to further adjust the AU p -value for introducing the selective inference p -value, denoted as SI. The theory and the algorithm of SI will be explained in Section 4 based on the geometric theory given in Section 3. After presenting the methods, we will revisit the phylogenetic inference in Section 4.3.

For developing the geometric theory in Sections 3 and 4, we formulate tree selection as the problem of regions (Efron, Halloran and Holmes, 1996; Efron and Tibshirani, 1998). For better understanding the geometric nature of the theory, the problem of regions is explained below for phylogenetic inference, although the algorithm is simple enough to

be implemented without understanding the theory. Considering the space of probability distributions (Amari and Nagaoka, 2007), the parametric models for trees are represented as manifolds in the space. The dataset (or the empirical distribution) can also be represented as a “data point” X in the space, and the ML estimates for trees are represented as projections to the manifolds. This is illustrated in the visualization of probability distributions of figure 3A using log-likelihood vectors of models (Shimodaira, 2001), where models are simply indicated as red lines from the origin; see Section 6.2 for details. This visualization may be called as *model map*. The point X is actually reconstructed as the minimum full model containing all the trees as submodels, and the Kullback-Leibler divergence between probability distributions is represented as the squared distance between points; see eq. (27). Computation of X is analogous to the Bayesian model averaging, but based on the ML method. For each tree, we can think of a region in the space so that this tree becomes the ML tree when X is included in the region. The regions for T1, T2 and T3 are illustrated in figure 3B, and the region for E2 is the union of these three regions.

As can be seen from the figure, X is very far from any of the tree models, suggesting that all the models are wrong; the likelihood ratio statistic for testing T1 against the full model is 113.4, which is highly significant as χ_8^2 (Shimodaira, 2001, Section 5). Instead of testing whether tree models are correct or not, we are going to test which model is better than the others. As you see, X is in the region for T1, meaning the model for T1 is better than those for the other trees, and we would like to know if it is *significantly better* or not. Quite similarly, X is in the region for E2 which consists of the three regions for T1, T2 and T3. This does not mean E2 is better than the other edges, because regions for edges overlap with each other, whereas regions for trees are disjoint. Some of the models for T1, T2 and T3 are better than those for T4, ..., T15 (actually T1 is better than the others), and we would like to know if they are *significantly better* or not. For convenience, observing X in the region for T1/E2, we state that it is *supported* by the dataset, and the significance is rephrased as T1/E2 is *significantly supported* in this paper.

3. Non-Selective Inference for the Problem of Regions

3.1. The Problem of Regions

For developing the theory, we consider $(m + 1)$ -dimensional multivariate normal random vector \mathbf{Y} with unknown mean vector $\boldsymbol{\mu} \in \mathbb{R}^{m+1}$ and the identity variance matrix \mathbf{I}_{m+1} :

$$\mathbf{Y} \sim N_{m+1}(\boldsymbol{\mu}, \mathbf{I}_{m+1}). \quad (4)$$

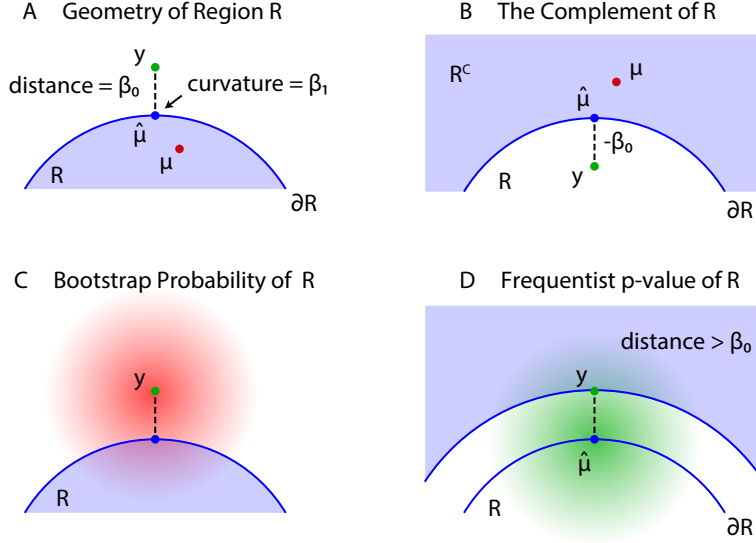


FIG 4. *Problem of regions.* (A) $\beta_0 > 0$ when $\mathbf{y} \in \mathcal{R}^C$, then select the null hypothesis $\boldsymbol{\mu} \in \mathcal{R}$. (B) $\beta_0 \leq 0$ when $\mathbf{y} \in \mathcal{R}$, then select the null hypothesis $\boldsymbol{\mu} \in \mathcal{R}^C$. (C) The bootstrap distribution of $\mathbf{Y}^* \sim N_{m+1}(\mathbf{y}, \mathbf{I}_{m+1})$ (red shaded distribution). (D) The null distribution of $\mathbf{Y} \sim N_{m+1}(\hat{\boldsymbol{\mu}}, \mathbf{I}_{m+1})$ (green shaded distribution).

Observing $\mathbf{Y} = \mathbf{y}$, we would like to test the null hypothesis $H_0 : \boldsymbol{\mu} \in \mathcal{R}$ against the alternative hypothesis $H_1 : \boldsymbol{\mu} \in \mathcal{R}^C$, where $\mathcal{R} \subset \mathbb{R}^{m+1}$ is a region of interest, and $\mathcal{R}^C = \mathbb{R}^{m+1} \setminus \mathcal{R}$ is the complement set. We can deal with arbitrary shape of \mathcal{R} in any $m \geq 0$ if it is represented as (29) in Section 6.3. This setting is called *problem of regions*, and the geometric theory for non-selective inference for slightly generalized settings (e.g., exponential family of distributions) has been discussed in Efron and Tibshirani (1998); Shimodaira (2004).

The problem of regions is well described by geometric quantities (figure 4). Let $\hat{\boldsymbol{\mu}}$ be the projection of \mathbf{y} to the boundary surface $\partial\mathcal{R}$ defined as

$$\hat{\boldsymbol{\mu}} = \arg \min_{\boldsymbol{\mu} \in \partial\mathcal{R}} \|\mathbf{y} - \boldsymbol{\mu}\|,$$

and β_0 be the *signed distance* defined as $\beta_0 = \|\mathbf{y} - \hat{\boldsymbol{\mu}}\| > 0$ for $\mathbf{y} \in \mathcal{R}^C$ and $\beta_0 = -\|\mathbf{y} - \hat{\boldsymbol{\mu}}\| \leq 0$ for $\mathbf{y} \in \mathcal{R}$; see figures 4A and B, respectively. A large β_0 indicates the evidence for rejecting $H_0 : \boldsymbol{\mu} \in \mathcal{R}$, but computation of p -value will also depend on the shape of \mathcal{R} . There should be many parameters for defining the shape, but we only need the *mean curvature* of $\partial\mathcal{R}$ at $\hat{\boldsymbol{\mu}}$, which represents how the surface curves. It is denoted as β_1 , and defined in (30).

Geometric quantities β_0 and β_1 of regions for trees (T1, ..., T105) and edges (E1, ...,

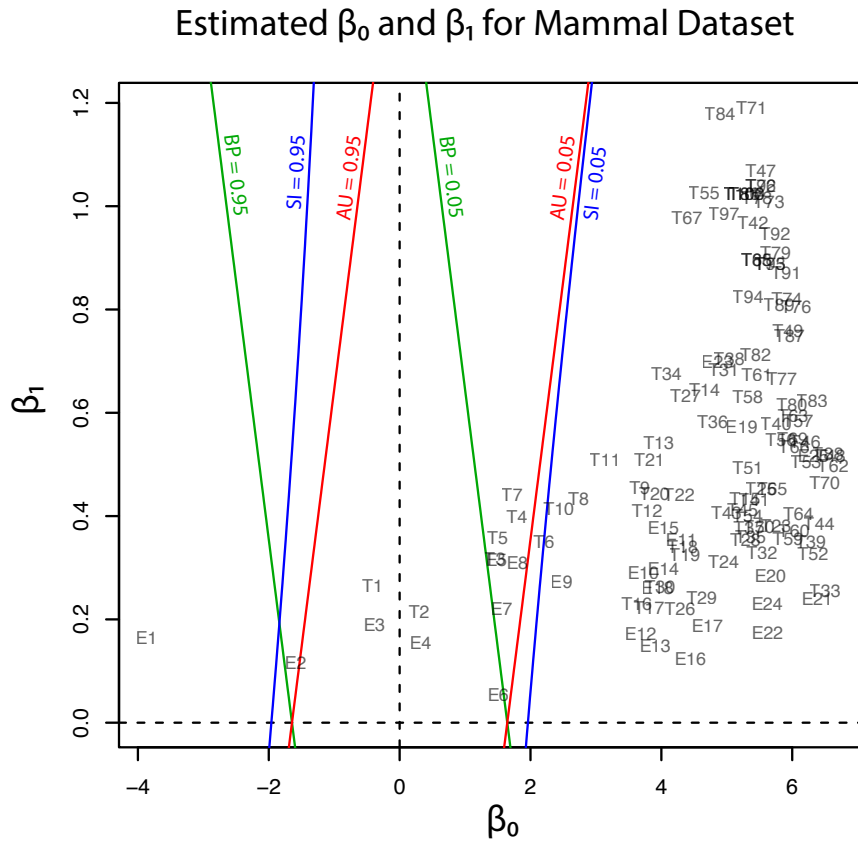


FIG 5. Geometric quantities of regions (β_0 and β_1) for trees and edges are estimated by the multiscale bootstrap method (Section 3.4). The three types of p-value (BP, AU, SI) are computed from β_0 and β_1 , and their contour lines are drawn at 0.05 and 0.95.

E25) are plotted in figure 5, and these values are also found in tables 1 and 2. Although the phylogenetic model of evolution for the molecular dataset $\mathcal{X}_n = (\mathbf{x}_1, \dots, \mathbf{x}_n)$ is different from the multivariate normal model (4) for \mathbf{y} , the multiscale bootstrap method of Section 3.4 estimates β_0 and β_1 using the non-parametric bootstrap probabilities (Section 6.1) with bootstrap replicates \mathcal{X}_n^* , for several values of sample size n' .

3.2. Bootstrap Probability

For simulating (4) from \mathbf{y} , we may generate replicates \mathbf{Y}^* from the bootstrap distribution (figure 4C)

$$\mathbf{Y}^* \sim N_{m+1}(\mathbf{y}, \mathbf{I}_{m+1}), \quad (5)$$

and define bootstrap probability (BP) of \mathcal{R} as the probability of \mathbf{Y}^* being included in the region \mathcal{R} :

$$\text{BP}(\mathcal{R}|\mathbf{y}) := P(\mathbf{Y}^* \in \mathcal{R}|\mathbf{y}). \quad (6)$$

$\text{BP}(\mathcal{R}|\mathbf{y})$ can be interpreted as the Bayesian posterior probability $P(\boldsymbol{\mu} \in \mathcal{R}|\mathbf{y})$, because, by assuming the flat prior distribution $\pi(\boldsymbol{\mu}) = \text{constant}$, the posterior distribution $\boldsymbol{\mu}|\mathbf{y} \sim N_{m+1}(\mathbf{y}, \mathbf{I}_{m+1})$ is identical to the distribution of \mathbf{Y}^* in (5). An interesting consequence of the geometric theory of Efron and Tibshirani (1998) is that BP can be expressed as

$$\text{BP}(\mathcal{R}|\mathbf{y}) \simeq \bar{\Phi}(\beta_0 + \beta_1), \quad (7)$$

where \simeq indicates the *second order asymptotic accuracy*, meaning that the equality is correct up to $O_p(n^{-1/2})$ with error of order $O_p(n^{-1})$; see Section 6.3. The model (4) reduces to (1) when $\partial\mathcal{R}$ is flat, where $\beta_0 = z$, $\beta_1 = 0$. Since BP is $P(Z^* \leq 0|z) = \bar{\Phi}(z)$ for $Z^* \sim N(z, 1)$, we have $\text{BP}(\mathcal{R}|\mathbf{y}) = \bar{\Phi}(\beta_0)$. For general \mathcal{R} , (7) adjusts the bias caused by β_1 .

BP of \mathcal{R}^C is closely related to BP of \mathcal{R} . From the definition,

$$\text{BP}(\mathcal{R}^C|\mathbf{y}) = 1 - \text{BP}(\mathcal{R}|\mathbf{y}) \simeq 1 - \bar{\Phi}(\beta_0 + \beta_1) = \bar{\Phi}(-\beta_0 - \beta_1). \quad (8)$$

The last expression also implies that the signed distance and the mean curvature of \mathcal{R}^C is $-\beta_0$ and $-\beta_1$, respectively; this relation is obtained by reversing the sign of v in (29).

3.3. Approximately Unbiased Test

Although $\text{BP}(\mathcal{R}|\mathbf{y})$ may work as a Bayesian confidence measure, we would like to have a frequentist confidence measure for testing $H_0 : \boldsymbol{\mu} \in \mathcal{R}$. Similar to (2), we define an

approximately unbiased (AU) p -value as

$$\text{AU}(\mathcal{R}|\mathbf{y}) := P(\beta_0(\mathbf{Y}) > \beta_0 \mid \boldsymbol{\mu} = \hat{\boldsymbol{\mu}}) = \text{BP}(\{\beta_0(\mathbf{Y}) > \beta_0\}|\hat{\boldsymbol{\mu}}), \quad (9)$$

where $\beta_0(\mathbf{Y})$ denotes the signed distance of \mathbf{Y} , and the probability is calculated for $\mathbf{Y} \sim N_{m+1}(\hat{\boldsymbol{\mu}}, \mathbf{I}_{m+1})$ as illustrated in figure 4D. The shape of the region $\{\beta_0(\mathbf{Y}) > \beta_0\}$ is very similar to the shape of \mathcal{R}^C ; the difference is in fact only $O_p(n^{-1})$. Let us think of a point \mathbf{y}' with signed distance $-\beta_0$ (shown as \mathbf{y} in figure 4B). Then we have

$$\text{AU}(\mathcal{R}|\mathbf{y}) \simeq \text{BP}(\mathcal{R}^C|\mathbf{y}') \simeq \bar{\Phi}(\beta_0 - \beta_1), \quad (10)$$

where the last expression is obtained by substituting $(-\beta_0, \beta_1)$ for (β_0, β_1) in (8). This formula computes AU from (β_0, β_1) . An intuitive interpretation of (10) is explained in Section 6.4.

We reject $H_0 : \boldsymbol{\mu} \in \mathcal{R}$ and take $H_1 : \boldsymbol{\mu} \in \mathcal{R}^C$, if $\text{AU}(\mathcal{R}|\mathbf{y}) < \alpha$. This test is approximately unbiased, because it controls the non-selective type-I error as

$$P(\text{AU}(\mathcal{R}|\mathbf{Y}) < \alpha \mid \boldsymbol{\mu} \in \partial\mathcal{R}) \simeq \alpha, \quad (11)$$

and the rejection probability increases as $\boldsymbol{\mu}$ moves away from \mathcal{R} , while it decreases as $\boldsymbol{\mu}$ moves into \mathcal{R} .

AU of \mathcal{R}^C is immediately obtained by substituting $(-\beta_0, -\beta_1)$, i.e., the geometric quantities of \mathcal{R}^C , for (β_0, β_1) in (10). This gives

$$\text{AU}(\mathcal{R}^C|\mathbf{y}) \simeq \bar{\Phi}(-\beta_0 + \beta_1) \simeq 1 - \text{AU}(\mathcal{R}|\mathbf{y}), \quad (12)$$

which is not surprising, because $\text{AU}(\mathcal{R}^C|\mathbf{y}) = 1 - \text{AU}(\mathcal{R}|\mathbf{y})$ is also obtained from the definition (9) by reversing the inequality. We reject $H_0 : \boldsymbol{\mu} \in \mathcal{R}^C$ and take $H_1 : \boldsymbol{\mu} \in \mathcal{R}$, if $\text{AU}(\mathcal{R}^C|\mathbf{y}) < \alpha$ or equivalently $\text{AU}(\mathcal{R}|\mathbf{y}) > 1 - \alpha$.

3.4. Multiscale Bootstrap

For estimating β_0 and β_1 from bootstrap probabilities, we consider a generalization of (5) as

$$\mathbf{Y}^* \sim N_{m+1}(\mathbf{y}, \sigma^2 \mathbf{I}_{m+1}), \quad (13)$$

for a variance $\sigma^2 > 0$, and define multiscale bootstrap probability of \mathcal{R} as

$$\text{BP}_{\sigma^2}(\mathcal{R}|\mathbf{y}) := P_{\sigma^2}(\mathbf{Y}^* \in \mathcal{R}|\mathbf{y}), \quad (14)$$

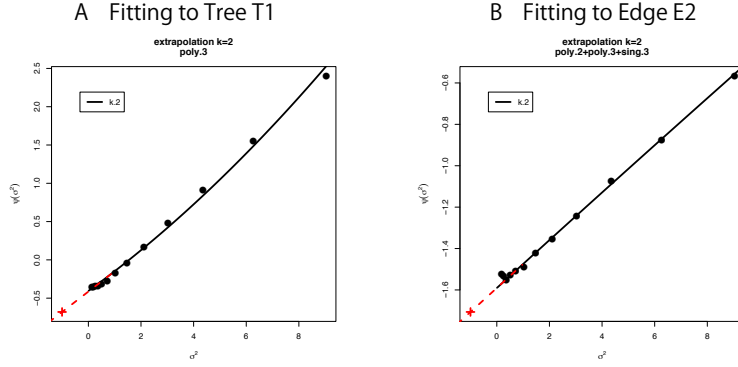


FIG 6. Multiscale bootstrap for (A) tree $T1$ and (B) edge $E2$. $\psi_{\sigma^2}(\mathcal{R}|\mathbf{y})$ is computed by the non-parametric bootstrap probabilities for several $\sigma^2 = n/n'$ values, then β_0 and β_1 are estimated as the intercept and the slope, respectively. See Section 6.5 for details.

where P_{σ^2} indicates the probability with respect to (13).

Although our theory is based on the multivariate normal model, the actual implementation of the algorithm uses the non-parametric bootstrap probabilities in Section 6.1. To fill the gap between the two models, we consider a non-linear transformation \mathbf{f}_n so that $\mathbf{y} = \mathbf{f}_n(\mathcal{X}_n)$ and $\mathbf{Y}^* = \mathbf{f}_n(\mathcal{X}_{n'}^*)$ satisfy (13) at least approximately. An example of \mathbf{f}_n is given in (25) for phylogenetic inference. Surprisingly, a specification of \mathbf{f}_n is *not required* for computing p -values, but we simply assume the existence of such a transformation. For phylogenetic inference, we compute the non-parametric bootstrap probabilities by (24) and substitute these values for (14) with $\sigma^2 = n/n'$.

For estimating β_0 and β_1 , we need to have a scaling law which explains how BP_{σ^2} depends on the scale σ . We rescale (13) by multiplying σ^{-1} so that $\sigma^{-1}\mathbf{Y}^* \sim N_{m+1}(\sigma^{-1}\mathbf{y}, \mathbf{I}_{m+1})$ has the variance $\sigma^2 = 1$. \mathbf{y} and \mathcal{R} are now rescaled by the factor σ^{-1} , which amounts to signed distance $\beta_0\sigma^{-1}$ and mean curvature $\beta_1\sigma$ (Shimodaira, 2004). Therefore, by substituting $(\beta_0\sigma^{-1}, \beta_1\sigma)$ for (β_0, β_1) in (7), we obtain

$$\text{BP}_{\sigma^2}(\mathcal{R}|\mathbf{y}) \simeq \bar{\Phi}(\beta_0\sigma^{-1} + \beta_1\sigma). \quad (15)$$

For better illustrating how BP_{σ^2} depends on σ^2 , we define

$$\psi_{\sigma^2}(\mathcal{R}|\mathbf{y}) := \sigma\bar{\Phi}^{-1}(\text{BP}_{\sigma^2}(\mathcal{R}|\mathbf{y})) \simeq \beta_0 + \beta_1\sigma^2. \quad (16)$$

We can estimate β_0 and β_1 as regression coefficients by fitting the linear model (16) in terms of σ^2 to the observed values of non-parametric bootstrap probabilities (figure 6). Interestingly, (10) is rewritten as $\text{AU}(\mathcal{R}|\mathbf{y}) \simeq \bar{\Phi}(\psi_{-1}(\mathcal{R}|\mathbf{y}))$ by formally letting $\sigma^2 = -1$ in the last expression of (16), meaning that AU corresponds to $n' = -n$. Although σ^2

should be positive in (15), we can think of negative σ^2 in $\beta_0 + \beta_1\sigma^2$. See Section 6.5 for details of model fitting and extrapolation to negative σ^2 .

4. Selective Inference for the Problem of Regions

4.1. Approximately Unbiased Test for Selective Inference

In order to argue selective inference for the problem of regions, we have to specify the selection event. Let us consider a selective region $\mathcal{S} \subset \mathcal{R}^{m+1}$ so that we perform the hypothesis testing only when $\mathbf{y} \in \mathcal{S}$. Terada and Shimodaira (2017) considered a general shape of \mathcal{S} , but here we treat only two special cases of $\mathcal{S} = \mathcal{R}^C$ and $\mathcal{S} = \mathcal{R}$; see Section 6.6. Our problem is formulated as follows. Observing $\mathbf{Y} = \mathbf{y}$ from the multivariate normal model (4), we first check whether $\mathbf{y} \in \mathcal{R}^C$ or $\mathbf{y} \in \mathcal{R}$. If $\mathbf{y} \in \mathcal{R}^C$ and we are interested in the null hypothesis $H_0 : \boldsymbol{\mu} \in \mathcal{R}$, then we may test it against the alternative hypothesis $H_1 : \boldsymbol{\mu} \in \mathcal{R}^C$. If $\mathbf{y} \in \mathcal{R}$ and we are interested in the null hypothesis $H_0 : \boldsymbol{\mu} \in \mathcal{R}^C$, then we may test it against the alternative hypothesis $H_1 : \boldsymbol{\mu} \in \mathcal{R}$. In this paper, the former case ($\mathbf{y} \in \mathcal{R}^C$, and so $\beta_0 > 0$) is called *outside mode*, and the latter case ($\mathbf{y} \in \mathcal{R}$, and so $\beta_0 \leq 0$) is called *inside mode*. We do not know which of the two modes of testing is performed until we observe \mathbf{y} .

Let us consider the outside mode $\mathbf{y} \in \mathcal{R}^C$, where $\beta_0 > 0$. Recalling that $p(z, c) = p(z)/\bar{\Phi}(c)$ in Section 1, we divide $\text{AU}(\mathcal{R}|\mathbf{y})$ by the selection probability to define a selective inference p -value as

$$\text{SI}(\mathcal{R}|\mathbf{y}) := \frac{P(\beta_0(\mathbf{Y}) > \beta_0 \mid \boldsymbol{\mu} = \hat{\boldsymbol{\mu}})}{P(\mathbf{Y} \in \mathcal{R}^C \mid \boldsymbol{\mu} = \hat{\boldsymbol{\mu}})} = \frac{\text{AU}(\mathcal{R}|\mathbf{y})}{\text{BP}(\mathcal{R}^C|\hat{\boldsymbol{\mu}})}. \quad (17)$$

From the definition, $\text{SI}(\mathcal{R}|\mathbf{y}) \in (0, 1)$, because $\{\beta_0(\mathbf{Y}) > \beta_0\} \subset \mathcal{R}^C$ for $\beta_0 > 0$. This p -value is computed from (β_0, β_1) by

$$\text{SI}(\mathcal{R}|\mathbf{y}) \simeq \frac{\bar{\Phi}(\beta_0 - \beta_1)}{\bar{\Phi}(-\beta_1)}, \quad (18)$$

where $\text{BP}(\mathcal{R}^C|\hat{\boldsymbol{\mu}}) = \bar{\Phi}(-\beta_1)$ is obtained by substituting $(0, \beta_1)$ for (β_0, β_1) in (8). An intuitive justification of (18) is explained in Section 6.4.

We reject $H_0 : \boldsymbol{\mu} \in \mathcal{R}$ and take $H_1 : \boldsymbol{\mu} \in \mathcal{R}^C$ if $\text{SI}(\mathcal{R}|\mathbf{y}) < \alpha$. This test is approximately unbiased, because it controls the selective type-I error as

$$P(\text{SI}(\mathcal{R}|\mathbf{Y}) < \alpha \mid \mathbf{Y} \in \mathcal{R}^C, \boldsymbol{\mu} \in \partial\mathcal{R}) \simeq \alpha, \quad (19)$$

and the rejection probability increases as $\boldsymbol{\mu}$ moves away from \mathcal{R} , while it decreases as $\boldsymbol{\mu}$ moves into \mathcal{R} .

Now we consider the inside mode $\boldsymbol{y} \in \mathcal{R}$, where $\beta_0 \leq 0$. SI of \mathcal{R}^C is obtained from (17) by exchanging the roles of \mathcal{R} and \mathcal{R}^C .

$$\text{SI}(\mathcal{R}^C|\boldsymbol{y}) = \frac{\text{AU}(\mathcal{R}^C|\boldsymbol{y})}{\text{BP}(\mathcal{R}|\hat{\boldsymbol{\mu}})} \simeq \frac{\bar{\Phi}(-\beta_0 + \beta_1)}{\bar{\Phi}(\beta_1)}. \quad (20)$$

We reject $H_0 : \boldsymbol{\mu} \in \mathcal{R}^C$ and take $H_1 : \boldsymbol{\mu} \in \mathcal{R}$, if $\text{SI}(\mathcal{R}^C|\boldsymbol{y}) < \alpha$. This is *not* equivalent to $\text{SI}(\mathcal{R}|\boldsymbol{y}) > 1 - \alpha$, because $\text{SI}(\mathcal{R}|\boldsymbol{y}) + \text{SI}(\mathcal{R}^C|\boldsymbol{y}) \neq 1$. For convenience, we define

$$\text{SI}'(\mathcal{R}|\boldsymbol{y}) := \begin{cases} \text{SI}(\mathcal{R}|\boldsymbol{y}) & \boldsymbol{y} \in \mathcal{R}^C \\ 1 - \text{SI}(\mathcal{R}^C|\boldsymbol{y}) & \boldsymbol{y} \in \mathcal{R} \end{cases} \quad (21)$$

so that $\text{SI}' > 1 - \alpha$ implies $\text{SI}(\mathcal{R}^C|\boldsymbol{y}) < \alpha$. In figure 5, tables 1 and 2, SI' is simply denoted as SI. We do not need to consider (21) for BP and AU, because $\text{BP}'(\mathcal{R}|\boldsymbol{y}) = \text{BP}(\mathcal{R}|\boldsymbol{y})$ and $\text{AU}'(\mathcal{R}|\boldsymbol{y}) = \text{AU}(\mathcal{R}|\boldsymbol{y})$ from (8) and (12).

4.2. Quick Computation of SI

We can compute SI from BP and AU. This will be useful for reanalyzing the results of previously published researches. Let us write $\text{BP} = \text{BP}(\mathcal{R}|\boldsymbol{y})$ and $\text{AU} = \text{AU}(\mathcal{R}|\boldsymbol{y})$. From (7) and (10), we have

$$\begin{aligned} \beta_0 &= \frac{1}{2} \left(\bar{\Phi}^{-1}(\text{BP}) + \bar{\Phi}^{-1}(\text{AU}) \right) \\ \beta_1 &= \frac{1}{2} \left(\bar{\Phi}^{-1}(\text{BP}) - \bar{\Phi}^{-1}(\text{AU}) \right). \end{aligned}$$

We can compute SI from β_0 and β_1 by (18) or (20). More directly, we may compute

$$\begin{aligned} \text{SI}(\mathcal{R}|\boldsymbol{y}) &= \frac{\text{AU}}{\bar{\Phi} \left\{ \frac{1}{2} \left(\bar{\Phi}^{-1}(\text{AU}) - \bar{\Phi}^{-1}(\text{BP}) \right) \right\}} \\ \text{SI}(\mathcal{R}^C|\boldsymbol{y}) &= \frac{1 - \text{AU}}{\bar{\Phi} \left\{ \frac{1}{2} \left(\bar{\Phi}^{-1}(\text{BP}) - \bar{\Phi}^{-1}(\text{AU}) \right) \right\}}. \end{aligned}$$

4.3. Revisiting the Phylogenetic Inference

Now we are ready for interpreting the analysis of Section 2. The question is: Which of mouse or human is closer to rabbit? The traditional view (Novacek, 1992) is actually

supporting E6, the clade of rabbit and mouse, which is consistent with T4, T5 and T7. Based on molecular analysis, Graur, Duret and Gouy (1996) strongly suggested that rabbit is closer to human than mouse, thus supporting E2, which is consistent with T1, T2 and T3. However, Halanych (1998) criticized it by pointing out that E2 is an artifact caused by the *long branch attraction* (LBA) between mouse and opossum. In addition, Shimodaira and Hasegawa (1999); Shimodaira (2002) suggested that T7 is not rejected by multiplicity adjusted tests. Shimodaira and Hasegawa (2005) showed that T7 becomes the ML tree by resolving the LBA using a larger dataset with more taxa. Although T1 is the ML tree based on the dataset with fewer taxa, T7 is presumably the true tree as indicated by later researches. With these observations in mind, we retrospectively interpret p -values in tables 1 and 2.

There are two modes of testing as defined in Section 4.1, and we will discuss these two modes separately, because properties of p -values depend on the mode. Let $K_{\text{true}} = K_{\text{all}} - K_{\text{select}}$ be the number of true null hypotheses, where $K_{\text{all}} = 105$ for trees and 25 for edges. In inside mode, we test $H_0 : \boldsymbol{\mu} \in \mathcal{R}^C$ against $H_1 : \boldsymbol{\mu} \in \mathcal{R}$ for $\mathbf{y} \in \mathcal{R}$ (i.e., $\beta_0 \leq 0$). This applies to the regions for T1, E1, E2 and E3, and they are *supported* by the dataset in the sense mentioned in the last paragraph of Section 2. For convenience, the null hypothesis is said like T1 is not true, and the alternative hypothesis is said like T1 is true. By testing the null hypotheses, we would like to know whether the alternative hypotheses are *significantly supported* or not. Noting $K_{\text{select}} = 1$ for trees and 3 for edges, selection bias can be very large in the sense that $K_{\text{select}}/K_{\text{all}} \approx 0$ for many taxa, and non-selective tests may lead to many false positives because $K_{\text{true}}/K_{\text{all}} \approx 1$. In outside mode, we test $H_0 : \boldsymbol{\mu} \in \mathcal{R}$ against $H_1 : \boldsymbol{\mu} \in \mathcal{R}^C$ for $\mathbf{y} \in \mathcal{R}^C$ (i.e., $\beta_0 > 0$). This applies to the regions for T2, ..., T105, and E4, ..., E25, and they are *not supported* by the dataset. For convenience, the null hypothesis is said like T2 is true, and the alternative hypothesis is said like T2 is not true. By testing the null hypotheses, we would like to know whether they are *rejected* or not. Noting $K_{\text{true}} = 1$ for trees and 3 for edges, selection bias is minor in the sense that $K_{\text{select}}/K_{\text{all}} \approx 1$ for many taxa, and non-selective tests may result in few false positives because $K_{\text{true}}/K_{\text{all}} \approx 0$. Selective inference is not much beneficial in outside mode.

Before examining p -values for some trees and edges, we look at the estimated geometric quantities in the tables. We confirm that the sign of β_0 is estimated correctly for all the trees and edges. The estimated β_1 values are all positive, indicating the regions are convex. This is not surprising, because the regions are expressed as intersections of half spaces at least locally (figure 3B).

Now we look at p -values in inside mode. (T1, E3) BP, AU, SI are all $p \leq 0.95$. This indicates that T1 and E3 are *not* significantly supported. We cannot claim anything definite. T1 is rarely significant for comparing many trees in practice. (E1) BP, AU, SI are all $p > 0.95$, indicating E1 is significantly supported. Since E1 is associated with the best 15 trees T1, ..., T15, some of them are significantly better than the rest of trees T16, ..., T105. Significance for edges is common in phylogenetics as well as in hierarchical clustering (Suzuki and Shimodaira, 2006). (E2) The results split for this presumably wrong edge. $AU > 0.95$ suggests E2 is significantly supported, whereas $BP, SI \leq 0.95$ are not significant. AU tends to violate the selective type-I error, leading to false positives or overconfidence in wrong trees/edges, whereas SI is approximately unbiased for the selected hypothesis. This overconfidence is explained by the inequality $AU > SI$ (meant SI' here) for $\mathbf{y} \in \mathcal{R}$, which is obtained by comparing (12) and (20). Therefore SI is preferable to AU in inside mode. BP is safer than AU in the sense that $BP < AU$ for $\beta_1 > 0$, but BP is not guaranteed for controlling anything in a frequentist sense. You can verify the two inequalities ($SI, BP < AU$) as relative positions of the contour lines at $p = 0.95$ in figure 5. The three p -values can be very different from each other for large β_1 .

Next we look at p -values in outside mode. (T2, E4, E6) BP, AU, SI are all $p \geq 0.05$. They are *not* rejected, and we cannot claim anything definite. (T8, T9, ..., T105, E9, ..., E25) BP, AU, SI are all $p < 0.05$. These trees and edges are rejected. (T7, E8) The results split for these presumably true tree and edge. $BP < 0.05$ suggests T7 and E8 are rejected, whereas $AU, SI \geq 0.05$ are not significant. BP tends to violate the type-I error, leading to false positives, whereas AU is approximately unbiased for hypotheses specified in advance (Shimodaira, 2002). Rejection of the true tree results in overconfidence in non-rejected wrong trees. This overconfidence of BP is explained by the inequality $BP < AU$ for $\beta_1 > 0$. Therefore BP should be avoided in outside mode. We can also show that $AU < SI$ for $\mathbf{y} \in \mathcal{R}^C$ by comparing (10) and (18). Since we chose to test $H_0 : \boldsymbol{\mu} \in \mathcal{R}$ after looking at $\mathbf{y} \in \mathcal{R}^C$, AU is not approximately unbiased for controlling the selective type-I error, whereas SI adjusts this selection bias. You can verify the two inequalities ($BP < AU < SI$) as relative positions of the contour lines at $p = 0.05$ in figure 5. AU and SI are similar, while BP is very different from AU and SI for large β_1 . It is arguable which of AU and SI is appropriate: AU is preferable to SI in tree selection, because there is no selection bias when all the candidate trees (formally including the ML tree) are tested in outside mode. In fact, the multiplicity of testing is controlled as $\text{FWER} = P(\text{reject any true null}) = P(\text{AU}(\mathcal{R}_{\text{true tree}}|\mathbf{Y}) < \alpha \mid \boldsymbol{\mu} \in \mathcal{R}_{\text{true tree}}) \leq \alpha$ because $K_{\text{true}} = 1$ for tree selection. The FWER is multiplied by $K_{\text{true}} \geq 1$ for edge selection, and

SI does not fix it either. Although edges are rarely tested in outside mode, AU may be used for screening purpose with a small α value such as α/K_{true} .

5. Conclusion

We have developed a new method for computing selective inference p -values from multi-scale bootstrap probabilities, and applied this new method to phylogenetics. Phylogenetic tree selection is formulated as the problem of regions. It is demonstrated through theory and a real-data analysis that selective inference (SI) p -value is in particular useful for testing selected edges (i.e., clades or clusters of species) to claim that they are supported significantly if $p > 1 - \alpha$. On the other hand, the previously proposed non-selective version of approximately unbiased (AU) p -value is still useful for testing candidate trees to claim that they are rejected if $p < \alpha$. This is the very first application of our general theory of selective inference, and it may be applied to other model selection problems, or more generally any selection problems.

6. Remarks

6.1. Bootstrap resampling of log-likelihoods

Non-parametric bootstrap is often time consuming for recomputing the ML estimates for bootstrap replicates. [Kishino, Miyata and Hasegawa \(1990\)](#) considered the resampling of estimated log-likelihoods (RELL) method for reducing the computation. Let $\mathcal{X}_n = (\mathbf{x}_1, \dots, \mathbf{x}_n)$ be the dataset of sample size n , where \mathbf{x}_t is the site-pattern of amino acids at site t for $t = 1, \dots, n$. By resampling \mathbf{x}_t from \mathcal{X}_n with replacement, we obtain a bootstrap replicate $\mathcal{X}_{n'}^* = (\mathbf{x}_1^*, \dots, \mathbf{x}_{n'}^*)$ of sample size n' . Although $n' = n$ for the ordinary bootstrap, we will use several $n' > 0$ values for the multiscale bootstrap. The parametric model of probability distribution for tree T_i is $p_i(\mathbf{x}; \boldsymbol{\theta}_i)$ for $i = 1, \dots, 105$, and the log-likelihood function is $\ell_i(\boldsymbol{\theta}_i; \mathcal{X}_n) = \sum_{t=1}^n \log p_i(\mathbf{x}_t; \boldsymbol{\theta}_i)$. Computation of the ML estimate $\hat{\boldsymbol{\theta}}_i = \arg \max_{\boldsymbol{\theta}_i} \ell_i(\boldsymbol{\theta}_i; \mathcal{X}_n)$ is time consuming, so we do not recalculate $\hat{\boldsymbol{\theta}}_i^* = \arg \max_{\boldsymbol{\theta}_i} \ell_i(\boldsymbol{\theta}_i; \mathcal{X}_{n'}^*)$ for bootstrap replicates. Define the site-wise log-likelihood at site t for tree T_i as

$$\xi_{ti} = \log p_i(\mathbf{x}_t; \hat{\boldsymbol{\theta}}_i), \quad t = 1, \dots, n, i = 1, \dots, 105, \quad (22)$$

so that the log-likelihood value for tree T_i is written as $\ell_i(\hat{\boldsymbol{\theta}}_i; \mathcal{X}_n) = \sum_{t=1}^n \xi_{ti}$. The bootstrap replicate of the log-likelihood value is approximated as

$$\ell_i(\hat{\boldsymbol{\theta}}_i^*; \mathcal{X}_{n'}^*) \approx \ell_i(\hat{\boldsymbol{\theta}}_i; \mathcal{X}_{n'}^*) = \sum_{t=1}^n w_t^* \xi_{ti}, \quad (23)$$

where w_t^* is the number of times \mathbf{x}_t appears in $\mathcal{X}_{n'}^*$. The accuracy of this approximation as well as the higher-order term is given in eqs. (4) and (5) of Shimodaira (2001). Once $\ell_i(\hat{\boldsymbol{\theta}}_i^*; \mathcal{X}_{n'}^*)$, $i = 1, \dots, 105$, are computed by (23), its ML tree is $T_{\hat{i}^*}$ with $\hat{i}^* = \arg \max_{i=1, \dots, 105} \ell_i(\hat{\boldsymbol{\theta}}_i^*; \mathcal{X}_{n'}^*)$.

The non-parametric bootstrap probability of tree T_i is obtained as follows. We generate B bootstrap replicates $\mathcal{X}_{n'}^{*b}$, $b = 1, \dots, B$. In this paper, we used $B = 10^5$. For each $\mathcal{X}_{n'}^{*b}$, the ML tree $T_{\hat{i}^{*b}}$ is computed by the method described above. Then we count the frequency that T_i becomes the ML tree in the B replicates. The non-parametric bootstrap probability is computed by

$$\text{BP}(T_i, n') = \#\{\hat{i}^{*b} = i, b = 1, \dots, B\} / B. \quad (24)$$

The non-parametric bootstrap probability of a edge is computed by summing $\text{BP}(T_i, n')$ over the associated trees.

An example of the transformation $\mathbf{Y}^* = \mathbf{f}_n(\mathcal{X}_{n'}^*)$ mentioned in Section 3.4 is

$$\mathbf{Y}^* = \mathbf{V}_n^{-1/2} \mathbf{L}_{n'}^*, \quad (25)$$

where $\mathbf{L}_{n'}^* = (1/n')(\ell_1^*, \dots, \ell_{105}^*)^T$ with $\ell_i^* = \ell_i(\hat{\boldsymbol{\theta}}_i^*; \mathcal{X}_{n'}^*)$ and \mathbf{V}_n is the variance matrix of \mathbf{L}_n^* . According to the approximation (23) and the central limit theorem, (13) holds well for sufficiently large n and n' with $m = 104$ and $\sigma^2 = n/n'$. It also follows from the above argument that $\text{var}(\ell_i^* - \ell_j^*) \approx (n'/n) \|\boldsymbol{\xi}_i - \boldsymbol{\xi}_j\|^2$, and thus the variance of log-likelihood difference is

$$\text{var}\left(\ell_i(\hat{\boldsymbol{\theta}}_i; \mathcal{X}_n) - \ell_j(\hat{\boldsymbol{\theta}}_j; \mathcal{X}_n)\right) \approx \|\boldsymbol{\xi}_i - \boldsymbol{\xi}_j\|^2, \quad (26)$$

which gives another insight into the visualization of Section 6.2, where the variance can be interpreted as the divergence between the two models; see eq. (27). When the two predictive distributions $p_i(\mathbf{x}; \hat{\boldsymbol{\theta}}_i)$, $p_j(\mathbf{x}; \hat{\boldsymbol{\theta}}_j)$ are close to each other, the higher-order term ignored in (26) becomes dominant, and there is a difficulty for deriving the limiting distribution of the log-likelihood difference in the model selection test (Shimodaira, 1997; Schennach and Wilhelm, 2017).

6.2. Visualization of Probability Models

For representing the probability distribution of tree T_i , we define $\boldsymbol{\xi}_i := (\xi_{1i}, \dots, \xi_{ni})^T \in \mathbb{R}^n$ from (22) for $i = 1, \dots, 15$. The idea behind the visualization of figure 3 is that locations of $\boldsymbol{\xi}_i$ in \mathbb{R}^n will represent locations of $p_i(\mathbf{x}; \hat{\boldsymbol{\theta}}_i)$ in the space of probability distributions. Let $D_{\text{KL}}(p_i \| p_j)$ be the Kullback-Leibler divergence between the two distributions. For sufficiently small $(1/n) \|\boldsymbol{\xi}_i - \boldsymbol{\xi}_j\|^2$, the squared distance in \mathbb{R}^n approximates n times Jeffreys divergence

$$\|\boldsymbol{\xi}_i - \boldsymbol{\xi}_j\|^2 \approx n \times \left(D_{\text{KL}}(p_i(\mathbf{x}; \hat{\boldsymbol{\theta}}_i) \| p_j(\mathbf{x}; \hat{\boldsymbol{\theta}}_j)) + D_{\text{KL}}(p_j(\mathbf{x}; \hat{\boldsymbol{\theta}}_j) \| p_i(\mathbf{x}; \hat{\boldsymbol{\theta}}_i)) \right) \quad (27)$$

for non-nested models (Shimodaira, 2001, Section 6). When a model p_0 is nested in p_i , it becomes $\|\boldsymbol{\xi}_i - \boldsymbol{\xi}_0\|^2 \approx 2n \times D_{\text{KL}}(p_i(\mathbf{x}; \hat{\boldsymbol{\theta}}_i) \| p_0(\mathbf{x}; \hat{\boldsymbol{\theta}}_0)) \approx 2 \times (\ell_i(\hat{\boldsymbol{\theta}}_i; \mathcal{X}_n) - \ell_0(\hat{\boldsymbol{\theta}}_0; \mathcal{X}_n))$. We explain three different visualizations of figure 7. There are only minor differences between the plots, and the visualization is not sensitive to the details.

For dimensionality reduction, we have to specify the origin $\mathbf{c} \in \mathbb{R}^n$ and consider vectors $\mathbf{a}_i := \boldsymbol{\xi}_i - \mathbf{c}$. A naive choice would be the average $\mathbf{c} = \sum_{i=1}^{15} \boldsymbol{\xi}_i / 15$. By applying PCA without centering and scaling (e.g., `prcomp` with option `center=FALSE`, `scale=FALSE` in R) to the matrix $(\mathbf{a}_1, \dots, \mathbf{a}_{15})$, we obtain the visualization of $\boldsymbol{\xi}_i$ as the axes (red arrows) of biplot in figure 7A.

For computing the “data point” X in figure 3, we need more models. Let tree T106 be the star topology with no internal branch (completely unresolved tree), and T107, \dots , T131 be partially resolved tree topologies with only one internal branch corresponding to E1, \dots , E25, whereas T1, \dots , T105 are fully resolved trees (bifurcating trees). Then define $\boldsymbol{\eta}_i := \boldsymbol{\xi}_{106+i}$, $i = 0, \dots, 25$. Now we take $\mathbf{c} = \boldsymbol{\eta}_0$ for computing $\mathbf{a}_i = \boldsymbol{\xi}_i - \boldsymbol{\eta}_0$ and $\mathbf{b}_i = \boldsymbol{\eta}_i - \boldsymbol{\eta}_0$. There is hierarchy of models: $\boldsymbol{\eta}_0$ is the submodel nested in all the other models, and $\boldsymbol{\eta}_1, \boldsymbol{\eta}_2, \boldsymbol{\eta}_3$, for example, are submodels of $\boldsymbol{\xi}_1$ (T1 includes E1, E2, E3). By combining these non-nested models, we can reconstruct a comprehensive model in which all the other models are nested as submodels (Shimodaira, 2001, eq. (10) in Section 5). The idea is analogous to reconstructing the full model $y = \beta_1 x_1 + \dots + \beta_{25} x_{25} + \epsilon$ of multiple regression from submodels $y = \beta_1 x_1 + \epsilon, \dots, y = \beta_{25} x_{25} + \epsilon$. Thus we call it as “full model” in this paper, and the ML estimate of the full model is indicated as the data point X ; it is also said “super model” in Shimodaira and Hasegawa (2005). Let $\mathbf{B} = (\mathbf{b}_1, \dots, \mathbf{b}_{25}) \in \mathbb{R}^{n \times 25}$ and $\mathbf{d} = (\|\mathbf{b}_1\|^2, \dots, \|\mathbf{b}_{25}\|^2)^T \in \mathbb{R}^{25}$, then the vector for the full model is computed approximately by

$$\mathbf{a}_X = \mathbf{B}(\mathbf{B}^T \mathbf{B})^{-1} \mathbf{d}. \quad (28)$$

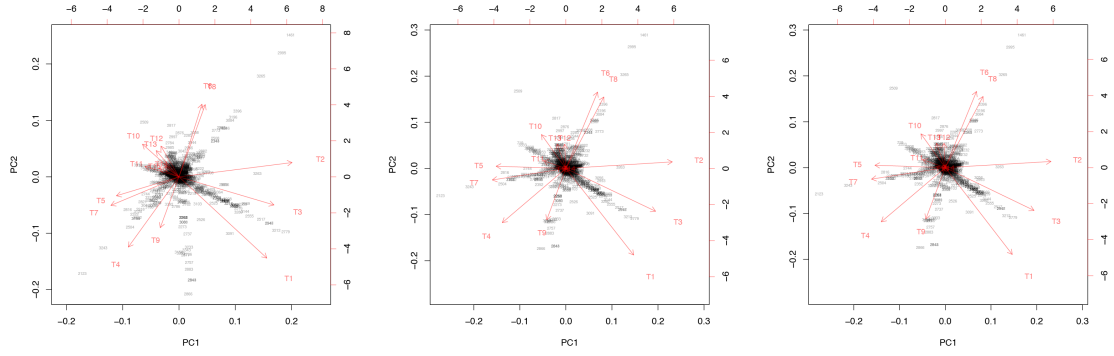


FIG 7. Three versions the visualization of probability distributions for the best 15 trees drawn using different sets of models. (A) Only the 15 bifurcating trees. (B) 15 bifurcating trees + 10 partially resolved trees + 1 star topology. This is the same plot as figure 3B. (C) 15 bifurcating trees + 1 star topology. Note that the origin is the simple average in A, while it is the star topology in B and C.

For the visualization of the best 15 trees, we may use only $\mathbf{b}_1, \dots, \mathbf{b}_{11}$, because they include E1 and two more edges from E2, \dots , E11. In figures 3 and 7B, we actually modified the above computation slightly so that the star topology T106 is replaced by T107, the partially resolved tree corresponding to E1 (T107 is also said star topology by treating clade (23) as a node), and the 10 partially resolved trees for E2, \dots , E11 are replaced by those for (E1,E2), \dots , (E1,E11), respectively; the origin becomes the maximal model nested in all the 15 trees, and X becomes the minimal full model containing all the 15 trees. Just before applying PCA in figure 7B, $\mathbf{a}_1, \dots, \mathbf{a}_{15}$ are projected to the space orthogonal to \mathbf{a}_X , so that the plot becomes the “top-view” of figure 3A with \mathbf{a}_X being at the origin.

In figure 7C, we attempted a even simpler computation without using ML estimates for partially resolved trees. We used $\mathbf{B} = (\mathbf{a}_1, \dots, \mathbf{a}_{15})$ and $\mathbf{d} = (\|\mathbf{a}_1\|^2, \dots, \|\mathbf{a}_{15}\|^2)^T$, and taking the largest 10 singular values for computing the inverse in (28). The orthogonal projection to \mathbf{a}_X is applied before PCA.

6.3. Asymptotic Theory of Smooth Surfaces

For expressing the shape of the region $\mathcal{R} \subset \mathbb{R}^{m+1}$, we use a local coordinate system $(\mathbf{u}, v) \in \mathbb{R}^{m+1}$ with $\mathbf{u} \in \mathbb{R}^m, v \in \mathbb{R}$. In a neighborhood of \mathbf{y} , the region is expressed as

$$\mathcal{R} = \{(\mathbf{u}, v) \mid v \leq -h(\mathbf{u}), \mathbf{u} \in \mathbb{R}^m\}, \quad (29)$$

where h is a smooth function; see Shimodaira (2008) for the theory of non-smooth surfaces. The boundary surface $\partial\mathcal{R}$ is expressed as $v = -h(\mathbf{u}), \mathbf{u} \in \mathbb{R}^m$. We can take the coordinates

so that $\mathbf{y} = (\mathbf{0}, \beta_0)$ (i.e., $\mathbf{u} = (0, \dots, 0)$ and $v = \beta_0$), and $h(\mathbf{0}) = 0$, $\partial h / \partial u_i|_{\mathbf{0}} = 0$, $i = 1, \dots, m$. The projection now becomes the origin $\hat{\boldsymbol{\mu}} = (\mathbf{0}, 0)$, and the signed distance is β_0 . The mean curvature of surface $\partial\mathcal{R}$ at $\hat{\boldsymbol{\mu}}$ is now defined as

$$\beta_1 = \frac{1}{2} \sum_{i=1}^m \frac{\partial^2 h(\mathbf{u})}{\partial u_i \partial u_i} \Big|_{\mathbf{0}}, \quad (30)$$

which is interpreted as the trace of the hessian matrix of h . When \mathcal{R} is convex at least locally in the neighborhood, all the eigenvalues of the hessian are non-negative, leading to $\beta_1 \geq 0$, whereas concave \mathcal{R} leads to $\beta_1 \leq 0$. In particular, $\beta_1 = 0$ when $\partial\mathcal{R}$ is flat (i.e., $h(\mathbf{u}) \equiv 0$).

Since the transformation $\mathbf{y} = \mathbf{f}_n(\mathcal{X}_n)$ depends on n , the shape of the region \mathcal{R} actually depends on n , although the dependency is implicit in the notation. As n goes larger, the standard deviation of estimates, in general, reduces at the rate $n^{-1/2}$. For keeping the variance constant in (4), we actually magnifying the space by the factor $n^{1/2}$, meaning that the boundary surface $\partial\mathcal{R}$ approaches flat as $n \rightarrow \infty$. More specifically, the magnitude of mean curvature is of order $\beta_1 = O_p(n^{-1/2})$. The magnitude of $\partial^3 h / \partial u_i \partial u_j \partial u_k$ and higher order derivatives is $O_p(n^{-1})$, and we ignore these terms in our asymptotic theory. For keeping $\boldsymbol{\mu} = O(1)$ in (4), we also consider the setting of ‘‘local alternatives’’, meaning that the parameter values approach a origin on the boundary at the rate $n^{-1/2}$.

6.4. Bridging the Problem of Regions to the Z-Test

Here we explain the problem of regions in terms of the z -test by bridging the multivariate problem of Section 3 to the 1-dimensional case of Section 1.

Ideal p -values are uniformly distributed over $p \in (0, 1)$ when the null hypothesis holds. In fact, $\text{AU}(\mathcal{R}|\mathbf{Y}) \sim U(0, 1)$ for $\boldsymbol{\mu} \in \partial\mathcal{R}$ as indicated in (11). The statistic $\text{AU}(\mathcal{R}|\mathbf{Y})$ may be called *pivotal* in the sense that the distribution does not change when $\boldsymbol{\mu} \in \partial\mathcal{R}$ moves on the surface. Here we ignore the error of $O_p(n^{-1})$, and consider only the second order asymptotic accuracy. From (10), we can write $\text{AU}(\mathcal{R}|\mathbf{Y}) \simeq \bar{\Phi}(\beta_0(\mathbf{Y}) - \beta_1(\mathbf{Y}))$, where the notation such as $\beta_0(\mathbf{Y})$ and $\beta_1(\mathbf{Y})$ indicates the dependency on \mathbf{Y} . Since $\beta_1(\mathbf{Y}) \simeq \beta_1(\mathbf{y}) = \beta_1$, we treat $\beta_1(\mathbf{Y})$ as a constant. Now we get the normal pivotal quantity (Efron, 1985) as $\bar{\Phi}^{-1}(\text{AU}(\mathcal{R}|\mathbf{Y})) = \beta_0(\mathbf{Y}) - \beta_1 \sim N(0, 1)$ for $\boldsymbol{\mu} \in \partial\mathcal{R}$. More generally, it becomes

$$\beta_0(\mathbf{Y}) - \beta_1 \sim N(\beta_0(\boldsymbol{\mu}), 1), \quad \boldsymbol{\mu} \in \mathbb{R}^{m+1}. \quad (31)$$

Let us look at the z -test in Section 1, and consider substitutions:

$$Z = \beta_0(\mathbf{Y}) - \beta_1, \quad \theta = \beta_0(\boldsymbol{\mu}), \quad c = -\beta_1. \quad (32)$$

The 1-dimensional model (1) is now equivalent to (31). The null hypothesis is also equivalent: $\theta \leq 0 \Leftrightarrow \beta_0(\boldsymbol{\mu}) \leq 0 \Leftrightarrow \boldsymbol{\mu} \in \mathcal{R}$. We can easily verify that AU corresponds to $p(z)$, because $p(z) = \bar{\Phi}(z) = \bar{\Phi}(\beta_0(\mathbf{y}) - \beta_1) \simeq \text{AU}(\mathcal{R}|\mathbf{y})$, which is expected from the way we obtained (31) above. Furthermore, we can derive SI from $p(z, c)$. First verify that the selection event is equivalent: $Z > c \Leftrightarrow \beta_0(\mathbf{Y}) - \beta_1 > -\beta_1 \Leftrightarrow \beta_0(\mathbf{Y}) > 0 \Leftrightarrow \mathbf{Y} \in \mathcal{R}^C$. Finally, we obtain SI as $p(z, c) = p(z)/\bar{\Phi}(c) \simeq \bar{\Phi}(\beta_0(\mathbf{y}) - \beta_1)/\bar{\Phi}(-\beta_1) \simeq \text{SI}(\mathcal{R}|\mathbf{y})$.

6.5. Model Fitting in Multiscale Bootstrap

We have used thirteen σ^2 values from 1/9 to 9 (equally spaced in log-scale). This range is relatively large, and we observe a slight deviation from the linear model $\beta_0 + \beta_1\sigma^2$ in figure 6. Therefore we fit other models to the observed values of ψ_{σ^2} as implemented in *scaleboot* package (Shimodaira, 2008). For example, poly. k model is $\sum_{i=0}^{k-1} \beta_i \sigma^{2i}$, and sing.3 model is $\beta_0 + \beta_1 \sigma^2 (1 + \beta_2 (\sigma - 1))^{-1}$. In figure 6A, poly.3 is the best model according to AIC (Akaike, 1974). In figure 6B, poly.2, poly.3, and sing.3 are combined by model averaging with Akaike weights. Then β_0 and β_1 are estimated from the tangent line to the fitted curve of ψ_{σ^2} at $\sigma^2 = 1$. In figure 6, the tangent line is drawn as red line for extrapolating ψ_{σ^2} to $\sigma^2 = -1$. Shimodaira (2008); Terada and Shimodaira (2017) considered the Taylor expansion of ψ_{σ^2} at $\sigma^2 = 1$ as a generalization of the tangent line for improving the accuracy of AU and SI.

In the implementation of *CONSEL* (Shimodaira and Hasegawa, 2001) and *pvclust* (Suzuki and Shimodaira, 2006), we use a narrower range of σ^2 values (ten σ^{-2} values: 0.5, 0.6, ..., 1.4). Only the linear model $\beta_0 + \beta_1\sigma^2$ is fitted there. The estimated β_0 and β_1 should be very close to those estimated from the tangent line described above. An advantage of using wider range of σ^2 in *scaleboot* is that the standard error of β_0 and β_1 will become smaller.

6.6. General Formula of Selective Inference

Let $\mathcal{H}, \mathcal{S} \subset \mathbb{R}^{m+1}$ be regions for the null hypothesis and the selection event, respectively. We would like to test the null hypothesis $H_0 : \boldsymbol{\mu} \in \mathcal{H}$ against the alternative $H_1 : \boldsymbol{\mu} \in \mathcal{H}^C$ conditioned on the selection event $\mathbf{y} \in \mathcal{S}$. Terada and Shimodaira (2017) gave a general formula of approximately unbiased p -value for this selective inference as

$$\text{SI}(\mathcal{H}|\mathcal{S}, \mathbf{y}) = \frac{\bar{\Phi}(\beta_0^{\mathcal{H}} - \beta_1^{\mathcal{H}})}{\bar{\Phi}(\beta_0^{\mathcal{S}} + \beta_0^{\mathcal{H}} - \beta_1^{\mathcal{H}})}, \quad (33)$$

where geometric quantities β_0, β_1 are defined for the regions \mathcal{H}, \mathcal{S} . We assumed that \mathcal{H} and \mathcal{S}^C are expressed as (29), and two surfaces $\partial\mathcal{H}, \partial\mathcal{S}$ are nearly parallel to each other

with tangent planes differing only $O_p(n^{-1/2})$. The last assumption always holds for (18), because $\partial\mathcal{R}$ and $\partial\mathcal{R}^C$ are identical and of course parallel to each other.

Here we explain why we have considered the special case of $\mathcal{S} = \mathcal{H}^C$ for phylogenetic inference. First, we suppose that the selection event satisfies $\mathcal{S} \subset \mathcal{H}^C$, because a reasonable test would not reject H_0 unless $\mathbf{y} \in \mathcal{H}^C$. Note that $\mathbf{y} \in \mathcal{S} \subset \mathcal{H}^C$ implies $0 \leq -\beta_0^{\mathcal{S}} \leq \beta_0^{\mathcal{H}}$. Therefore, $\beta_0^{\mathcal{H}} + \beta_0^{\mathcal{S}} \geq 0$ leads to

$$\text{SI}(\mathcal{H}|\mathcal{S}, \mathbf{y}) \geq \text{SI}(\mathcal{H}|\mathbf{y}), \quad (34)$$

where $\text{SI}(\mathcal{H}|\mathbf{y}) := \text{SI}(\mathcal{H}|\mathcal{H}^C, \mathbf{y})$ is obtained from (33) by letting $\beta_0^{\mathcal{H}} + \beta_0^{\mathcal{S}} = 0$ for $\mathcal{S} = \mathcal{H}^C$. The p -value $\text{SI}(\mathcal{H}|\mathcal{S}, \mathbf{y})$ becomes smaller as \mathcal{S} grows, and $\mathcal{S} = \mathcal{H}^C$ gives the smallest p -value, leading to the most powerful selective test. Therefore the choice $\mathcal{S} = \mathcal{H}^C$ is preferable to any other choice of selection event satisfying $\mathcal{S} \subset \mathcal{H}^C$. This kind of property is mentioned in Fithian, Sun and Taylor (2014) as the monotonicity of selective error in the context of “data curving”.

Let us see how these two p -values differ for the case of E2 by specifying $\mathcal{H} = \mathcal{R}_{\text{E2}}^C$ and $\mathcal{S} = \mathcal{R}_{\text{T1}}$. In this case, the two surfaces $\partial\mathcal{H}, \partial\mathcal{S}$ may not be very parallel to each other, thus violating the assumption of $\text{SI}(\mathcal{H}|\mathcal{S}, \mathbf{y})$, so we only intend to show the potential difference between the two p -values. The geometric quantities are $\beta_0^{\mathcal{H}} = -\beta_0^{\text{E2}} = 1.59$, $\beta_1^{\mathcal{H}} = -\beta_1^{\text{E2}} = -0.12$, $\beta_0^{\mathcal{S}} = \beta_0^{\text{T1}} = -0.41$; the p -values are calculated using more decimal places than shown. SI of E2 conditioned on selecting T1 is

$$\text{SI}(\mathcal{H}|\mathcal{S}, \mathbf{y}) = \frac{\bar{\Phi}(1.59 + 0.12)}{\bar{\Phi}(-0.41 + 1.59 + 0.21)} = 0.448,$$

and it is very different from SI of E2 conditioned on selecting E2

$$\text{SI}(\mathcal{H}|\mathbf{y}) = \frac{\bar{\Phi}(1.59 + 0.12)}{\bar{\Phi}(0.12)} = 0.097,$$

where $\text{SI}'(\mathcal{R}_{\text{E2}}^C|\mathbf{y}) = 1 - \text{SI}(\mathcal{R}_{\text{E2}}^C|\mathbf{y}) = 0.903$ is shown in table 2. As you see, $\text{SI}(\mathcal{H}|\mathbf{y})$ is easier to reject H_0 than $\text{SI}(\mathcal{H}|\mathcal{S}, \mathbf{y})$.

6.7. Selective Inference of Lasso Regression

Selective inference is considered for the variable selection of regression analysis. Here, we deal with prostate cancer data (Stamey et al., 1989) in which we predict the level of prostate-specific antigen (PSA) from clinical measures. The dataset is available in the R package *ElemStatLearn* (Halvorsen, 2015). We consider a linear model to the log of PSA

(lpsa), with 8 predictors such as the log prostate weight (`lweight`), `age`, and so on. All the variables are standardized to have zero mean and unit variance.

The goal is to provide the valid selective inference for the partial regression coefficients of the selected variables by lasso (Tibshirani, 1996). Let n and p be the number of observations and the number of predictors. $\hat{\mathbf{M}}$ is the set of selected variables, and $\hat{\mathbf{s}}$ represents the signs of the selected regression coefficients. We suppose that regression responses are distributed as $\mathbf{Y} \sim N(\boldsymbol{\mu}, \tau^2 \mathbf{I}_n)$ where $\boldsymbol{\mu} \in \mathbb{R}^n$ and $\tau > 0$. Let e_i be the i th residual. Resampling the scaled residuals σe_i ($i = 1, \dots, n$) with several values of scale σ^2 , we can apply the multiscale bootstrap method described in Section 4 for the selective inference in the regression problem. Here, we note that the target of the inference is the true partial regression coefficients:

$$\boldsymbol{\beta} = (\mathbf{X}^T \mathbf{X})^{-1} \mathbf{X}^T \boldsymbol{\mu},$$

where $\mathbf{X} \in \mathbb{R}^{n \times p}$ is the design matrix. We compute four types of intervals with confidence level $1 - \alpha = 0.95$ for selected variable j . $[L_j^{\text{ordinary}}, U_j^{\text{ordinary}}]$ is the non-selective confidence interval obtained via t -distribution. $[L_j^{\text{model}}, U_j^{\text{model}}]$ is the selective confidence interval under the selected model proposed by Lee et al. (2016) and Tibshirani et al. (2016), which is computed by `fixedLassoInf` with `type="full"` in R package *selectiveInference* (Tibshirani et al., 2017). By extending the method of $[L_j^{\text{model}}, U_j^{\text{model}}]$, we also computed $[L_j^{\text{variable}}, U_j^{\text{variable}}]$, which is the selective confidence interval under the selection event that variable j is selected. These three confidence intervals are exact, in the sense that

$$\begin{aligned} P\left(\beta_j \in [L_j^{\text{ordinary}}, U_j^{\text{ordinary}}]\right) &= 1 - \alpha, & P\left(\beta_j \in [L_j^{\text{model}}, U_j^{\text{model}}] \mid \hat{\mathbf{M}}, \hat{\mathbf{s}}\right) &= 1 - \alpha, \\ P\left(\beta_j \in [L_j^{\text{variable}}, U_j^{\text{variable}}] \mid j \in \hat{\mathbf{M}}, \hat{s}_j\right) &= 1 - \alpha. \end{aligned}$$

Note that the selection event $\{j \in \hat{\mathbf{M}}, \hat{s}_j\}$ can be represented as a union of polyhedra on \mathbb{R}^n , and thus, according to the polyhedral lemma (Lee et al., 2016; Tibshirani et al., 2016), we can compute a valid confidence interval $[L_j^{\text{variable}}, U_j^{\text{variable}}]$. However, this computation is prohibitive for $p > 10$, because all the possible combinations of models with variable j are considered. Therefore, we compute its approximation $[\hat{L}_j^{\text{variable}}, \hat{U}_j^{\text{variable}}]$ by the multiscale bootstrap method of Section 4 with much faster computation even for larger p .

We set $\lambda = 10$ as the penalty parameter of lasso, and the following model and signs were selected:

$$\hat{\mathbf{M}} = \{\text{lcavol}, \text{lweight}, \text{lbph}, \text{svi}, \text{pgg45}\}, \quad \hat{\mathbf{s}} = (+, +, +, +, +).$$

The confidence intervals are shown in figure 1. For adjusting the selection bias, the three confidence intervals of selective inference are longer than the ordinary confidence inter-

val. Comparing $[L_j^{\text{model}}, U_j^{\text{model}}]$ and $[L_j^{\text{variable}}, U_j^{\text{variable}}]$, the latter is shorter, and would be preferable. This is because the selection event of the latter is less restrictive as $\{\hat{M}, \hat{s}\} \subseteq \{j \in \hat{M}, \hat{s}_j\}$; see Section 6.6 for the reason why larger selection event is better. Finally, we verify that $[\hat{L}_j^{\text{variable}}, \hat{U}_j^{\text{variable}}]$ approximates $[L_j^{\text{variable}}, U_j^{\text{variable}}]$ very well.

Conflict of Interest Statement

The authors declare that the research was conducted in the absence of any commercial or financial relationships that could be construed as a potential conflict of interest.

Author Contributions

HS and YT developed the theory of selective inference. HS programmed the multiscale bootstrap software and conducted the phylogenetic analysis. YT conducted the lasso analysis. HS wrote the manuscript. All authors have approved the final version of the manuscript.

Funding

This research was supported in part by JSPS KAKENHI Grant (16H02789 to HS, 16K16024 to YT).

Acknowledgments

The authors appreciate the feedback from the audience of seminar talk of HS at Department of Statistics, Stanford University. The authors are grateful to Masami Hasegawa for his insightful comments on phylogenetic analysis of mammal species.

Data Availability Statement

The datasets analyzed for this study can be found in the software package *scaleboot* (Shimodaira, 2019).

References

ADACHI, J. and HASEGAWA, M. (1996). Model of amino acid substitution in proteins encoded by mitochondrial DNA. *J. Mol. Evol.* **42** 459–468.

- AKAIKE, H. (1974). A new look at the statistical model identification. *Automatic Control, IEEE Transactions on* **19** 716–723.
- AMARI, S.-I. and NAGAOKA, H. (2007). *Methods of information geometry* **191**. American Mathematical Soc.
- BURNHAM, K. P. and ANDERSON, D. R. (2002). *Model selection and multimodel inference: a practical information-theoretic approach*. Springer.
- COX, D. R. (1962). Further results on tests of separate families of hypotheses. *Journal of the Royal Statistical Society. Series B (Methodological)* **24** 406–424.
- EFRON, B. (1979). Bootstrap Methods: Another Look At the Jackknife. *Annals of Statistics* **7** 1–26.
- EFRON, B. (1984). Comparing non-nested linear models. *Journal of the American Statistical Association* **79** 791–803.
- EFRON, B. (1985). Bootstrap Confidence Intervals for a Class of Parametric Problems. *Biometrika* **72** 45–58.
- EFRON, B., HALLORAN, E. and HOLMES, S. (1996). Bootstrap confidence levels for phylogenetic trees. *Proc. Natl. Acad. Sci. USA* **93** 13429–13434.
- EFRON, B. and TIBSHIRANI, R. (1998). The problem of regions. *Annals of Statistics* **26** 1687–1718.
- FELSENSTEIN, J. (1981). Evolutionary Trees from DNA Sequences: A Maximum Likelihood Approach. *J. Mol. Evol.* **17** 368–376.
- FELSENSTEIN, J. (1985). Confidence limits on phylogenies: an approach using the bootstrap. *Evolution* **39** 783–791.
- FITHIAN, W., SUN, D. and TAYLOR, J. (2014). Optimal inference after model selection. *arXiv preprint arXiv:1410.2597*.
- GRAUR, D., DURET, L. and GOUY, M. (1996). Phylogenetic position of the order Lagomorpha (rabbits, hares and allies). *Nature* **379** 333.
- HALANYCH, K. M. (1998). Lagomorphs misplaced by more characters and fewer taxa. *Systematic Biology* **47** 138–146.
- HALVORSEN, K. (2015). ElemStatLearn: Data Sets, Functions and Examples from the Book: “The Elements of Statistical Learning, Data Mining, Inference, and Prediction” by Trevor Hastie, Robert Tibshirani and Jerome Friedman. *R package*. [<https://CRAN.R-project.org/package=ElemStatLearn>].
- KISHINO, H. and HASEGAWA, M. (1989). Evaluation of the maximum likelihood estimate of the evolutionary tree topologies from DNA sequence data, and the branching order in Hominoidea. *J. Mol. Evol.* **29** 170–179.

- KISHINO, H., MIYATA, T. and HASEGAWA, M. (1990). Maximum likelihood inference of protein phylogeny and the origin of chloroplasts. *J. Mol. Evol.* **30** 151–160.
- KONISHI, S. and KITAGAWA, G. (2008). *Information criteria and statistical modeling*. Springer Science & Business Media.
- LEE, J. D., SUN, D. L., SUN, Y. and TAYLOR, J. E. (2016). Exact post-selection inference, with application to the lasso. *Annals of Statistics* **44** 907–927.
- LINHART, H. (1988). A test whether two AICs differ significantly. *South African Statist. J.* **22** 153–161.
- NOVACEK, M. J. (1992). Mammalian phylogeny: shaking the tree. *Nature* **356** 121–125.
- POSADA, D. and BUCKLEY, T. R. (2004). Model selection and model averaging in phylogenetics: advantages of Akaike information criterion and Bayesian approaches over likelihood ratio tests. *Systematic biology* **53** 793–808.
- ROSENTHAL, R. (1979). The file drawer problem and tolerance for null results. *Psychological bulletin* **86** 638–641.
- SCHENNACH, S. M. and WILHELM, D. (2017). A simple parametric model selection test. *Journal of the American Statistical Association* **112** 1663–1674.
- SHIMODAIRA, H. (1997). Assessing the error probability of the model selection test. *Annals of the Institute of Statistical Mathematics* **49** 395–410.
- SHIMODAIRA, H. (1998). An application of multiple comparison techniques to model selection. *Annals of the Institute of Statistical Mathematics* **50** 1–13.
- SHIMODAIRA, H. (2000). Improving predictive inference under covariate shift by weighting the log-likelihood function. *Journal of Statistical Planning and Inference* **90** 227–244.
- SHIMODAIRA, H. (2001). Multiple comparisons of log-likelihoods and combining nonnested models with applications to phylogenetic tree selection. *Communications in Statistics-Theory and Methods* **30** 1751–1772.
- SHIMODAIRA, H. (2002). An approximately unbiased test of phylogenetic tree selection. *Systematic Biology* **51** 492–508.
- SHIMODAIRA, H. (2004). Approximately unbiased tests of regions using multistep-multiscale bootstrap resampling. *The Annals of Statistics* **32** 2616–2641.
- SHIMODAIRA, H. (2008). Testing regions with nonsmooth boundaries via multiscale bootstrap. *Journal of Statistical Planning and Inference* **138** 1227–1241.
- SHIMODAIRA, H. (2019). scaleboot: Approximately Unbiased P-Values via Multiscale Bootstrap. *R package version 1.0-0*. [<https://CRAN.R-project.org/package=scaleboot>].
- SHIMODAIRA, H. and HASEGAWA, M. (1999). Multiple comparisons of log-likelihoods

- with applications to phylogenetic inference. *Molecular Biology and Evolution* **16** 1114–1116.
- SHIMODAIRA, H. and HASEGAWA, M. (2001). CONSEL: for assessing the confidence of phylogenetic tree selection. *Bioinformatics* **17** 1246–1247.
- SHIMODAIRA, H. and HASEGAWA, M. (2005). Assessing the uncertainty in phylogenetic inference. In *Statistical Methods in Molecular Evolution*, (R. Nielsen, ed.). *Statistics for Biology and Health* 463–493. Springer.
- SHIMODAIRA, H. and MAEDA, H. (2018). An information criterion for model selection with missing data via complete-data divergence. *Annals of the Institute of Statistical Mathematics* **70** 421–438.
- STAMEY, T., KABALIN, J., JOHNSTONE, I., FREIHA, F., REDWINE, E. and YANG, N. (1989). Prostate specific antigen in the diagnosis and treatment of adenocarcinoma of the prostate II. Radical prostatectomy treated patients. *Journal of Urology* **16** 1076–1083.
- SUZUKI, R. and SHIMODAIRA, H. (2006). Pvclust: an R package for assessing the uncertainty in hierarchical clustering. *Bioinformatics* **22** 1540–1542.
- TAYLOR, J. and TIBSHIRANI, R. (2015). Statistical learning and selective inference. *Proceedings of the National Academy of Sciences of the United States of America* **112** 7629–7634.
- TERADA, Y. and SHIMODAIRA, H. (2017). Selective inference for the problem of regions via multiscale bootstrap. *arXiv preprint arXiv:1711.00949*.
- TIAN, X. and TAYLOR, J. (2018). Selective inference with a randomized response. *The Annals of Statistics* **46** 679–710.
- TIBSHIRANI, R. (1996). Regression shrinkage and selection via the lasso. *Journal of the Royal Statistical Society. Series B (Methodological)* **58** 267–288.
- TIBSHIRANI, R., TAYLOR, J., LOCKHART, R. and TIBSHIRANI, R. (2016). Exact Post-Selection Inference for Sequential Regression Procedures. *Journal of the American Statistical Association* **111** 600–620.
- TIBSHIRANI, R., TIBSHIRANI, R., TAYLOR, J., LOFTUS, J. and REID, S. (2017). selectiveInference: Tools for Post-Selection Inference. *R package version 1.2.4*. [<https://CRAN.R-project.org/package=selectiveInference>].
- VUONG, Q. H. (1989). Likelihood ratio tests for model selection and non-nested hypotheses. *Econometrica* **57** 307–333.
- YANG, Z. (1996). Among-site rate variation and its impact on phylogenetic analyses. *Trends in Ecol. & Evol.* **11** 367–372.

YANG, Z. (1997). PAML: a program package for phylogenetic analysis by maximum likelihood. *Comput. Appl. Biosci.* **13** 555-556.